RESEARCH ARTICLE

COLOR WILEY

The location of optimal object colors with more than two transitions

Scott A. Burns [ORCID]

Department of Industrial and Enterprise Systems Engineering, University of Illinois at Urbana-Champaign, Urbana, Illinois

Correspondence
Scott A. Burns, Department of Industrial and Enterprise Systems Engineering, University of Illinois at Urbana-Champaign, Urbana, IL 61801.
Email: scottallenburns@gmail.com

Abstract

The chromaticity diagram associated with the 1931 2° CIE color-matching functions is shown to be slightly non-convex. While having no impact on practical colorimetric computations, the non-convexity does have a significant impact on the shape of some optimal object color reflectance distributions located on the outer surface of the object color solid. Instead of the usual two-transition Schrödinger form, many optimal colors exhibit higher transition counts. A linear programming formulation is developed and is used to locate where these higher-transition optimal object colors reside on the object color solid surface. The regions of higher-transition count appear to have a point-symmetric, complementary structure. The high-transition behavior is shown to be largely absent in more modern color-matching functions, such as the recent "physiologically-relevant" color-matching functions transformed from cone fundamentals.

KEYWORDS
color-matching functions, linear programming, MacAdam limits, optimal object colors, Schrödinger colors

1 | INTRODUCTION

The color-matching functions (CMFs), when plotted as a set of three-dimensional vectors in tristimulus space, form an origin-vertexed cone enveloping all possible colors. Nested within this cone is the object color solid (OCS). It contains all "object colors" that can be produced by a nonfluorescent reflecting surface (ie, having a spectral reflectance distribution between 0 and 1), under the action of some specified illuminant. The outer surface of the OCS contains the "optimal object colors." Historically, the optimal colors are believed to be associated with rectangular spectral reflectance distributions having only values of 0 and 1 and at most two sudden transitions, known as Schrödinger colors.[1] This belief has been echoed in color science publications for many decades.[2-8]

West and Brill showed that one condition for all optimal colors to have the Schrödinger form is that the

chromaticity diagram (the so-called horseshoe diagram) be convex.[9] Most historic proofs of optimal colors having the Schrödinger form assume this convexity, either explicitly or implicitly.

Recently, Davis demonstrated that the CIE 1931 CMFs produce a non-convex chromaticity diagram.[10] He did this by measuring external angles around the chromaticity diagram using a specialized software package for color calculations written in R language, called colorSpec. He also presented a careful and precise statement of West and Brill's theorem and other related concepts, presented in lengthy mathematical form.

This article is directed more to the color scientist with a background in numerical methods instead of formal mathematics; the first part of this article will demonstrate the non-convexity of the chromaticity diagram using only a single MATLAB function. This non-convexity is very slight and has no impact on practical colorimetric

computations. It does, however, have a significant impact on the shape of some optimal object color reflectance distributions. Instead of the usual two-transition Schrödinger form, many optimal colors exhibit higher transition counts. A linear programming (LP) approach will be developed and be used to compute the reflectance distribution of optimal object colors, located anywhere on the OCS surface. It will be used to map regions where these higher-transition optimal colors reside on the OCS surface. An interesting complementary point-symmetry of the regions is observed.

Next, an analysis will reveal what portions of the chromaticity diagram are most responsible for the high-transition optimal object colors. Although the far blue and red ends of the diagram exhibit more severe non-convexities than elsewhere on the diagram, it will be demonstrated that the two ends have little influence on the production of high-transition optimal colors. An experiment will then be presented to "convexify" the CMFs through very slight perturbations of the color-matching values. This convexification succeeds in eliminating much, but not all, of the high-transition optimal object colors.

Finally, a similar analysis will be applied to the more recent "physiologically-relevant" CMFs transformed from cone fundamentals.[11] It will be demonstrated that although these CMFs also exhibit a slight degree of non-convexity, the prevalence of higher-transition optimal object colors is very minimal and is readily eliminated by the convexification process.

2 | CONVEXITY OF THE CHROMATICITY DIAGRAM

Here, we are considering the 1931 2° CIE Standard Colorimetric Observer Data (CMFs) that span 360 to 830 nm in 1 nm intervals.[11,12] We designate this 471×3 matrix with the symbol A. The chromaticity coordinates associated with A are found by dividing each row of A by the row sum. The first two columns are then identified as x and y chromaticity coordinates. In MATLAB this is accomplished with the statement $xy = A(:,1:2)./\text{sum}(A,2);$, where xy is a 471×2 matrix of chromaticity coordinates, producing the well-known "horseshoe" chromaticity diagram.

We now use the notion of a convex hull to assess the convexity of the chromaticity diagram. When applied to a discrete set of points in two dimensions, the convex hull is the smallest convex polygon that contains all of the points. If it turns out that any of the chromaticity coordinates of the horseshoe reside in the interior of the convex hull, then the horseshoe is not convex.

The convex hull is generated in MATLAB with the statement $k = \text{convhull}(xy)$. The vector k contains the indices

of rows of xy that form the convex hull boundary. It turns out that only 161 of the 471 rows of xy contribute to this boundary. Figure 1 depicts graphically where they are. The black dots are those that form the convex hull boundary and the red dots are those that fall inside of it.

Close examination of one of the red dots (figure inset) shows that the horseshoe polygon (solid black line) falls slightly inside the convex hull polygon (blue dashed line) in some areas. There are two main regions of non-convexity: several large pockets of wavelengths above 574 nm, and another segment running 435 to 453 nm. There are also many pockets of non-convexity at both extreme ends of the visible range.

The non-convexity persists with lower-resolution versions of the 1 nm CMFs. Figure 2 shows the non-convexity of 5 and 10 nm versions of CMFs that are commonly used in colorimetric computations. The red dots indicate that the non-convexity is present here as well.

This non-convexity is extremely small. In chromaticity space units, the horseshoe and convex hull polygons are only about 0.00005 units apart in the Figure 1 inset. This very small difference will have no practical impact on typical colorimetric calculations. It turns out, however, that it does have a significant impact on
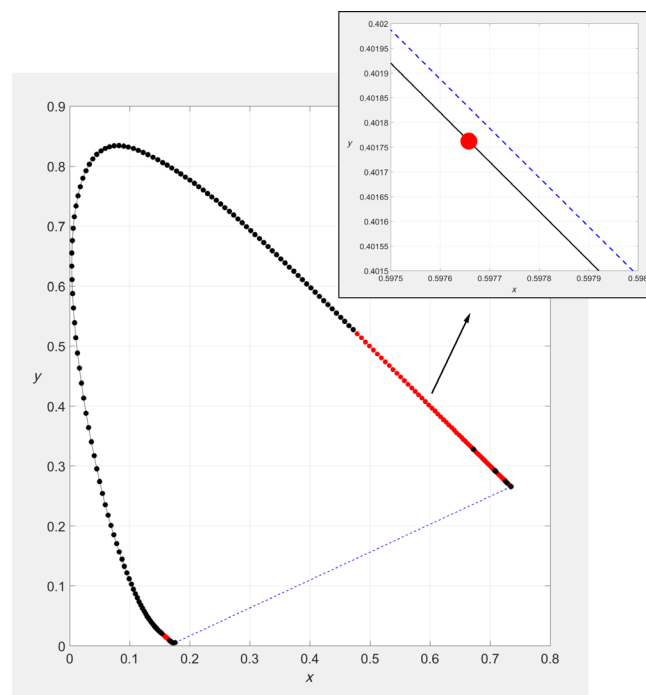

FIGURE 1 Chromaticity diagram (black solid line) and convex hull enveloping it (blue dashed line). Red dots are points on chromaticity diagram that fall slightly inside the convex hull, indicating a slight non-convexity of the horseshoe for portions above 574 nm and also a small portion running 435 to 453 nm
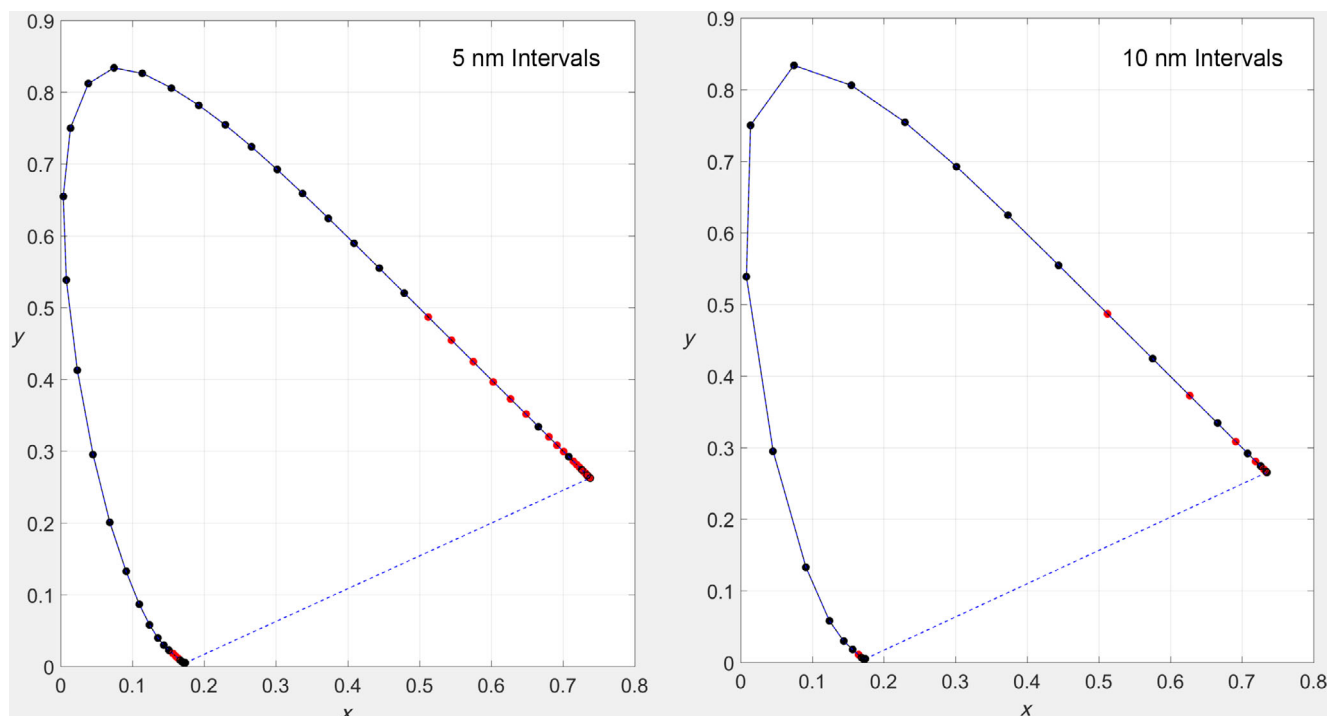
FIGURE 2 Convex hull analysis of lower-resolution versions of the 1 nm color-matching functions, having 5 nm wavelength intervals (left) and 10 nm intervals (right). Red dots show chromaticity coordinates falling slightly inside the convex hull boundary

the shape of optimal object colors, as discussed in the next sections.

3 | COMPUTING OPTIMAL OBJECT COLOR REFLECTANCE CURVES

The standard approach to characterizing the OCS is to start with two-transition Schrödinger reflectance curves and map them into tristimulus space to form the boundary of the solid.[2-5,13] An alternate approach is to make no assumption of the shape of the optimal reflectance curve, but seek points on the surface of the OCS by optimization methods. In this article, we follow the latter approach using LP. Historically, LP has been used in colorimetric calculations to compute metamer mismatch volumes,[14-17] to design illuminants to achieve desired rendering effects,[18] and to compute subtractive mixture recipes for colorants based on the Kubelka-Munk theory.[19-21]

The idea of using LP to identify the OCS surface is not new. In his 1969 article on limits of metamerism (ie, metamer mismatch volumes), Allen mentions in passing (without any details) that LP could be used to compute MacAdam limits (optimal object colors).[14] Ohta and Wyszecki repeat Allen's claim in their 1975 article on metamer mismatch volumes, but only go so far as to state that it would be achieved with a simplified version of

some of the equations they present.[15] In 2010, Li et al explicitly use LP to determine the shape of cross-sections of the OCS by first identifying key locations on each cross section by LP, and then by using LP repeatedly to fill in the curves between these key locations.[22] Although their LP formulation directly computes the shape of the reflectance curves as a by-product of the computation, the focus of their article is instead on identifying the shape of the OCS in tristimulus space. They apparently did not encounter (or perhaps notice) any cases where the two-transition assumption was violated (other than inevitable artifacts of discretization at the two-transition locations, which they did mention).

The LP presented in this article uses only one basic colorimetric equation:

$$XYZ_W = A_W' \, \rho. \tag{1}$$

In the above equation, XYZ_W is a 3×1 vector of illuminant-W-referenced tristimulus values, and ρ is an $n \times 1$ vector of reflectance values (0-1), where n is the number of wavelength intervals used to discretize continuous spectral distributions over the visible range. Matrix A_W is an $n \times 3$ matrix of illuminant-W-referenced CMFs, computed as $\bar{W}A$, where $\bar{W}$ is an $n \times n$ matrix with illuminant W on the main diagonal and zeros elsewhere. Prime denotes matrix transpose. As mentioned in Section 2, matrix A is an $n \times 3$ array of CMFs by columns, $A =$

$[\bar{x}, \bar{y}, \bar{z}]$. It is assumed that the illuminant has been normalized so that the scalar product $\bar{y}' \cdot W$ equals 100. For the standard 1931 2° CIE standard CMFs with 1 nm resolution, n is 471.

Note that the reflective/transmissive version of tristimulus values are being used here (as opposed to the emissive version), so all tristimulus values are referenced to an illuminant, hence the W subscript. Even though different subscripts may be used to identify special tristimulus values in this article, it is understood that all of them are W-referenced. For example, the white point, XYZ_{wp} is the tristimulus triplet formed as the three row sums of A_W' (three column sums of A_W).

Figure 3 presents a cut-away view of the interior of the OCS. Four key locations are identified, (a) the white point, XYZ_{wp}, (b) the 50% gray halfway point between the origin and the white point, $XYZ_{50\%} = XYZ_{wp}/2$, (c) an arbitrary point within the OCS, XYZ_{targ}, which defines a direction with respect to $XYZ_{50\%}$, and (4) the point of intersection of a ray in that direction with the OCS outer surface, XYZ_{opt}.

A spherical coordinate system is established, centered at $XYZ_{50\%}$. Every XYZ_{opt} on the surface is associated with a unique (θ, φ) pair. The spherical coordinate system will come in handy in a subsequent section, when it comes time to plot a dense array of optimal color data as viewed from the interior of the OCS.
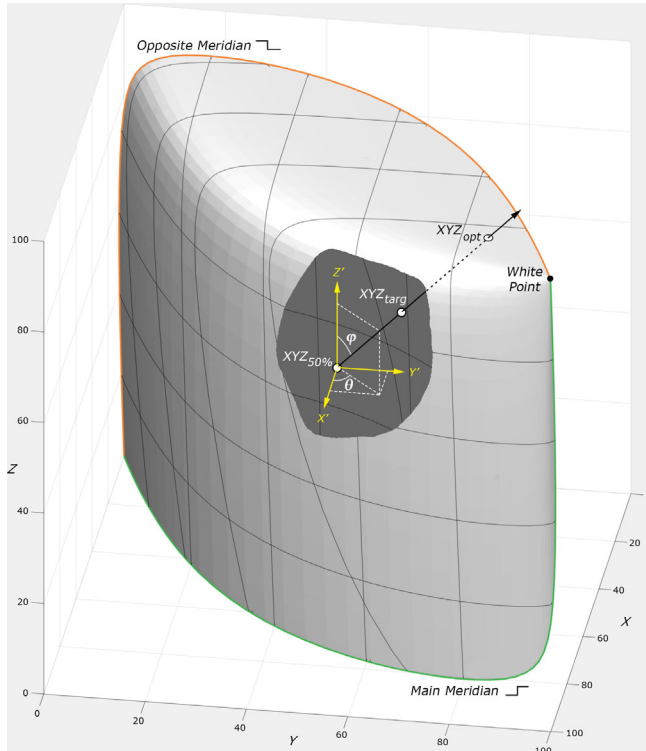

FIGURE 3 An object color solid with key locations identified

Consider the vector $XYZ_{targ} - XYZ_{50\%}$. When this vector is based at $XYZ_{50\%}$, it points in the direction of the ray shown in Figure 3. Next, consider a scalar, c, which serves to magnify the vector and locate an arbitrary point, XYZ, along the ray:

$$XYZ = XYZ_{50\%} + c(XYZ_{targ} - XYZ_{50\%}). \quad (2)$$

Substituting for XYZ using Equation (1), we now have an equation in terms of our unknowns, ρ and c. We seek to maximize c to move as far along the ray as possible, while constraining ρ to be between 0 and 1:

$$\begin{aligned} \max_{\rho, c} \quad & c \\ s.t. \quad & A_W' \rho = XYZ_{50\%} + c(XYZ_{targ} - XYZ_{50\%}) \\ & 0 \le \rho \le 1. \end{aligned} \quad (3)$$

This is a linear program. To solve this LP with MATLAB's "linprog" function, it needs to be recast in standard form:

$$\begin{aligned} \min_{x} \quad & f'x \\ s.t. \quad & A_{eq}x = b_{eq} \\ & x_{lb} \le x \le x_{ub}, \end{aligned} \quad (4)$$

where f, x, b_{eq}, x_{lb}, and x_{ub} are all vectors and A_{eq} is a matrix. This recasting of Equation 3 is accomplished by concatenating ρ and c into a single 472×1 vector and by minimizing $-c$.

$$\begin{aligned} \min_{\rho, c} \quad & -c \\ s.t. \quad & \left[A_W' | XYZ_{50\%} - XYZ_{targ} \right] \begin{Bmatrix} \rho \\ c \end{Bmatrix} = XYZ_{50\%} \\ & 0 \le \rho \le 1. \end{aligned} \quad (5)$$

The following MATLAB statements produce the optimal color reflectance distribution, ρ, corresponding to a point on the surface of the OCS that is the intersection of a ray emanating from $XYZ_{50\%}$, passing through XYZ_{targ}:

```
>> options = optimoptions('linprog', 'Algorithm',
'dual-simplex',...
 'OptimalityTolerance', 1e-9, 'ConstraintTolerance',
3e-9);
>> x = linprog([zeros(471,1);-1], [],[], [Aw',XYZ50-
XYZtarg], XYZ50,...
 [zeros(471,1);-Inf], [ones(471,1);Inf], options);
>> rho = x(1:471);
```

The two tolerances used internally by the LP solver are tightened up considerably. These values were determined

experimentally to avoid premature termination of the LP. Note that the MATLAB Optimization Toolbox is required for function linprog.

The vast majority of reflectance curves generated by this LP will have the expected two-transition structure. For example, using a target of $XYZ_{\text{targ}} = [10; 40; 30]$, the LP gives the reflectance shown on the left side of Figure 4. In some cases, however, more than two transitions are obtained. For example, if the target is changed to $XYZ_{\text{targ}} = [49.1; 40.3; 25.0]$, a four-transition reflectance curve is produced, as shown on the right side of Figure 4.

It is natural to question the higher-transition result. Is it just an artifact of the LP solution process? Is it really on the outer surface of the OCS? In other words, is there a two-transition solution along the same ray that is even farther from $XYZ_{50\%}$, which would make the high-transition solution an interior point of the OCS, and not optimal? The LP solution process involves pivots into and out of an active basis, using tolerances to decide if optimality conditions have been numerically satisfied. Is it possible that the higher-transition solutions are just barely suboptimal points that happen to satisfy the optimality conditions numerically within the specified tolerances? These issues will be addressed in Section 5, but first, a survey of how often and where the high-transition LP solutions occur will be presented.

4 | A MAP OF HIGH-TRANSITION LP SOLUTIONS

Figure 3 presented a spherical coordinate system centered at $XYZ_{50\%}$. A second rectangular coordinate system was also shown in that figure, defined as $(X', Y', Z') = (X,$ $Y, Z) - XYZ_{50\%}$. Suppose we wish to visualize the OCS surface by placing our viewpoint at $XYZ_{50\%}$ and directing our view either up or down the Z' axis. Figure 5 shows two polar plots of how we can arrange a mapping of the spherical coordinate system, in both cases, placing the X' axis running to the right. The left plot in Figure 5 visualizes the upper half of the OCS and the right plot visualizes the lower half.

We are now able to create a high-resolution bitmapped graphic by superimposing a rectangular lattice over each polar plot. The lattice points correspond to the pixels of a bitmapped image, and each pixel has a corresponding spherical coordinate pair, (θ, φ). We can formulate an LP for each pixel by defining $XYZ_{\text{targ}} = XYZ_{50\%} + [\sin(\varphi) \cos(\theta); \sin(\varphi) \sin(\theta); \cos(\varphi)]$. Figure 6 presents a color-coded summary of transition count of the LP solution associated with each pixel's XYZ_{targ}.

Several notable features stand out. First, it is evident that the vast majority of optimal colors have the two-transition Schrödinger form (the black and gray regions). Second, it appears that there are two regions of higher-transition optimal colors that are mirror images of one another. The region in the upper half are all type II-like, having reflectance of 1 everywhere except for several pockets of 0 values. Conversely, the region in the lower half are all type I-like, having 0 reflectance everywhere except for several pockets of 1 values. Another way to interpret this is that the complement of a higher-transition color is a color of the same transition count, but of the opposite type. A line connecting the two passes through $XYZ_{50\%}$ (point symmetry).

Certainly, there are two-transition object colors in the same directions as the higher-transition colors in Figure 6. How do they compare? The next section examines that question.
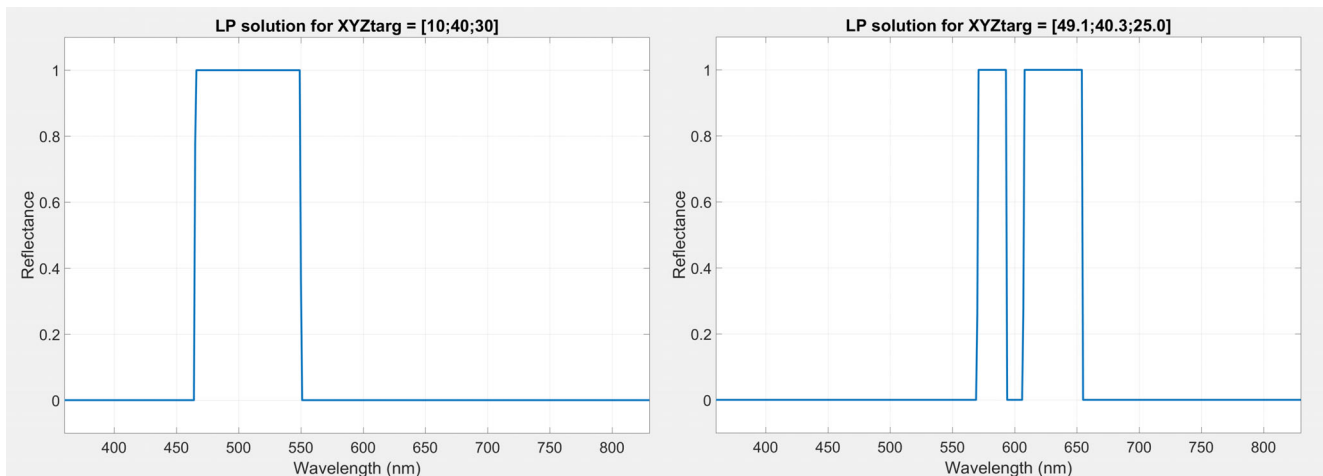

FIGURE 4 Reflectance curves produced by the linear programming for two different targets
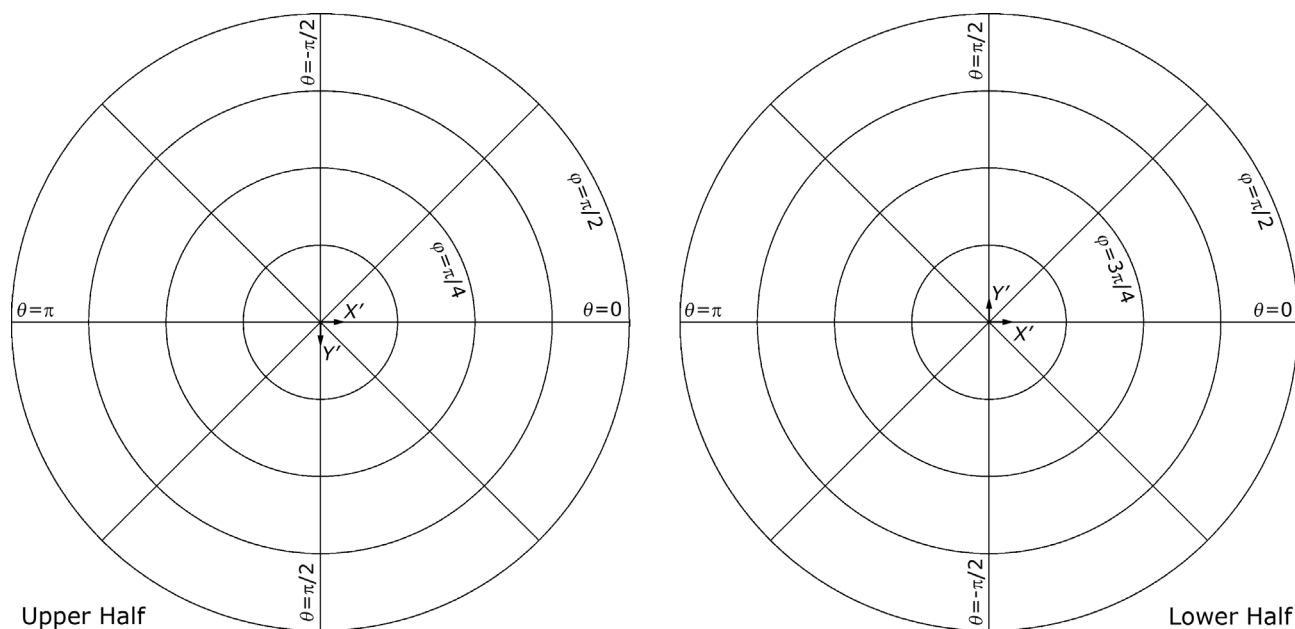
FIGURE 5 Polar mapping for upper and lower halves of object color solid

5 | ARE SOME SCHRÖDINGER COLORS SUBOPTIMAL?

The short answer appears to be yes, but only because of the slight non-convexity of the 1931 2° CIE Standard Colorimetric Observer Data. To demonstrate this, another computational experiment that parallels that shown in Figure 6 was performed, this time using each XYZ_{targ} to identify the two-transition color along the associated ray. This was accomplished using the MATLAB code that was presented in an article by Masaoka and Berns.[23] Its original purpose was to compute "optimal metamers" for Logvinenko's "object color space."[24] Here, it is adapted to compute only the two-transition part.[*]

By computing the distance from $XYZ_{50\%}$ to the tristimulus values of both the two-transition color and the high-transition color, both measured along the same ray, a comparison can be made. In all cases, the high-transition color was found to be slightly farther away from $XYZ_{50\%}$ than the two-transition color was. Figure 7 summarizes this difference graphically. Only the top half is shown, as the bottom half is again a point symmetric copy.

The gray region is where the LP solution gives a two-transition color, which matches the two-transition color returned by the Masaoka & Berns code. In those cases, the distances from $XYZ_{50\%}$ to each of the two, measured along the same direction from $XYZ_{50\%}$, match to machine floating point tolerance. In regions of higher transition count, however, the difference in distances is 10 *orders of magnitude* greater than machine floating point noise and

6 *orders of magnitude* greater than the LP optimality tolerances. Thus, the LP solutions obtained are not the result of numerical noise or optimality tolerances, but are distinct solutions located beyond the two-transition Schrödinger colors. In other words, the two-transition colors (in the regions where the LP gives higher-transition optimal colors) are suboptimal and fall somewhat inside the OCS volume.

6 | EFFECT OF CHANGING CMFS RESOLUTION

In Section 2, it was shown that the 1931 2° CIE CMFs retain non-convexity at other wavelength interval sizes. Here, we examine one specific point on the OCS surface and how the LP high-transition optimal color and two-transition color (from the Masaoka & Berns code) are affected by resolution of the CMFs. Figure 8 shows the two solutions for wavelength resolutions of 0.1, 1, 5, and 10 nm. The black line is the two-transition reflectance curve and the blue region is the LP optimal reflectance curve (Note that both are bar plots, one is filled in blue and the other is only outlined.). The small image inset into each of the four plots shows the transition count distribution as computed from the CMFs with the various wavelength interval sizes. It uses the same color coding as shown in Figure 6. Even at 10 nm intervals, the high-transition behavior persists. The small white dot in each plot shows where the two reflectance plots are located on the OCS surface.
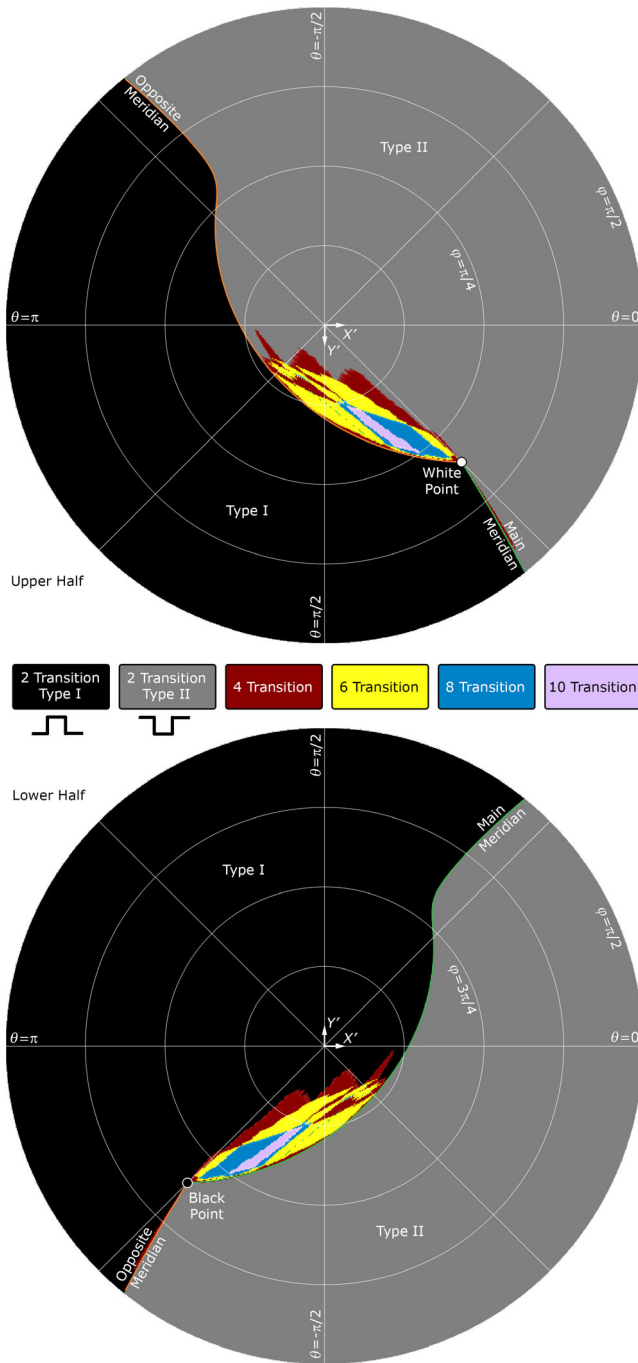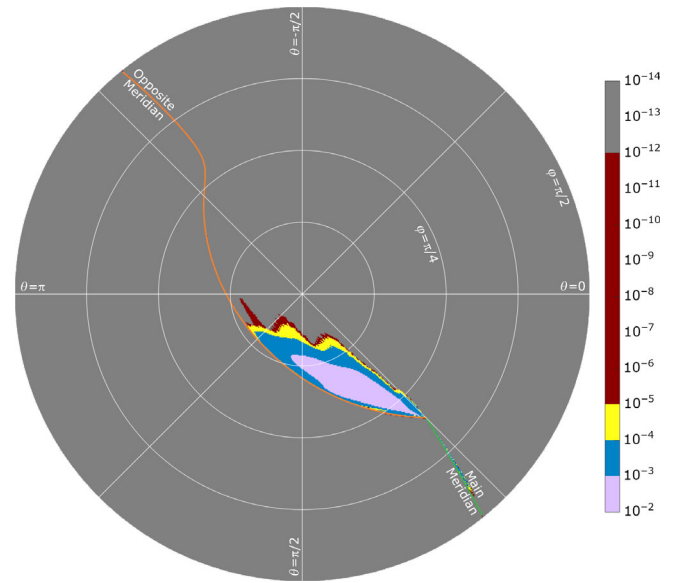
FIGURE 7 Difference in distances to the linear programming solutions and to the two-transition solutions, measured from $XYZ_{50\%}$, both along the same ray

FIGURE 6 A view of the top and bottom halves of the object color solid as viewed from the 50% gray point, looking in the $+Z'/-Z'$ directions

this should be interpreted is that the "true" transition points fall somewhere within the finite width of the wavelength interval. Li et al noticed this same artifact in their 2010 article, and came to the same conclusion.[22]

As mentioned in Section 5, the difference in tristimulus values between the LP solution and the two-transition solution is very small. For example, for the 1 nm case shown in Figure 8, we have the following numerical values:

$$\theta = 1.478858 \text{ rad}, \quad \varphi = 0.371322 \text{ rad}, \quad XYZ_{\text{targ}} = \begin{Bmatrix} 50.03731 \\ 50.36132 \\ 50.94838 \end{Bmatrix}$$

$$XYZ_{\text{LPsoln}} = \begin{Bmatrix} 51.79069 \\ 69.37875 \\ 99.99523 \end{Bmatrix}, \quad XYZ_{\text{two-trans}} = \begin{Bmatrix} 51.79066 \\ 69.37828 \\ 99.99402 \end{Bmatrix}$$

Difference in distance from $XYZ_{50\%} = 1.29 \times 10^{-3}$

(6)

The reflectance distributions all show magnitudes at the transition points that are between 0 and 1. This is an artifact of the discretization of the CMFs. Since both the LP and the Masaoka & Berns code have constraints that require the reflectance curve to have an associated tristimulus value triplet that exactly matches a specified value, the only way to satisfy this match is to allow the transition points to have intermediate values. The way

7 | OTHER ILLUMINANTS

So far, all results presented are for an equal-energy illuminant. Here, we examine how other illuminants affect the results. Five high-chroma Munsell colors were selected, 5R 5/14, 5Y 8/16, 5G 7/10, 5B 6/10, and 5P 4/12, and an illuminant was created with the same chromaticity, using a "smoothest" reflectance reconstruction technique.[25-26]

FIGURE 8 The effect of different color-matching functions wavelength interval size
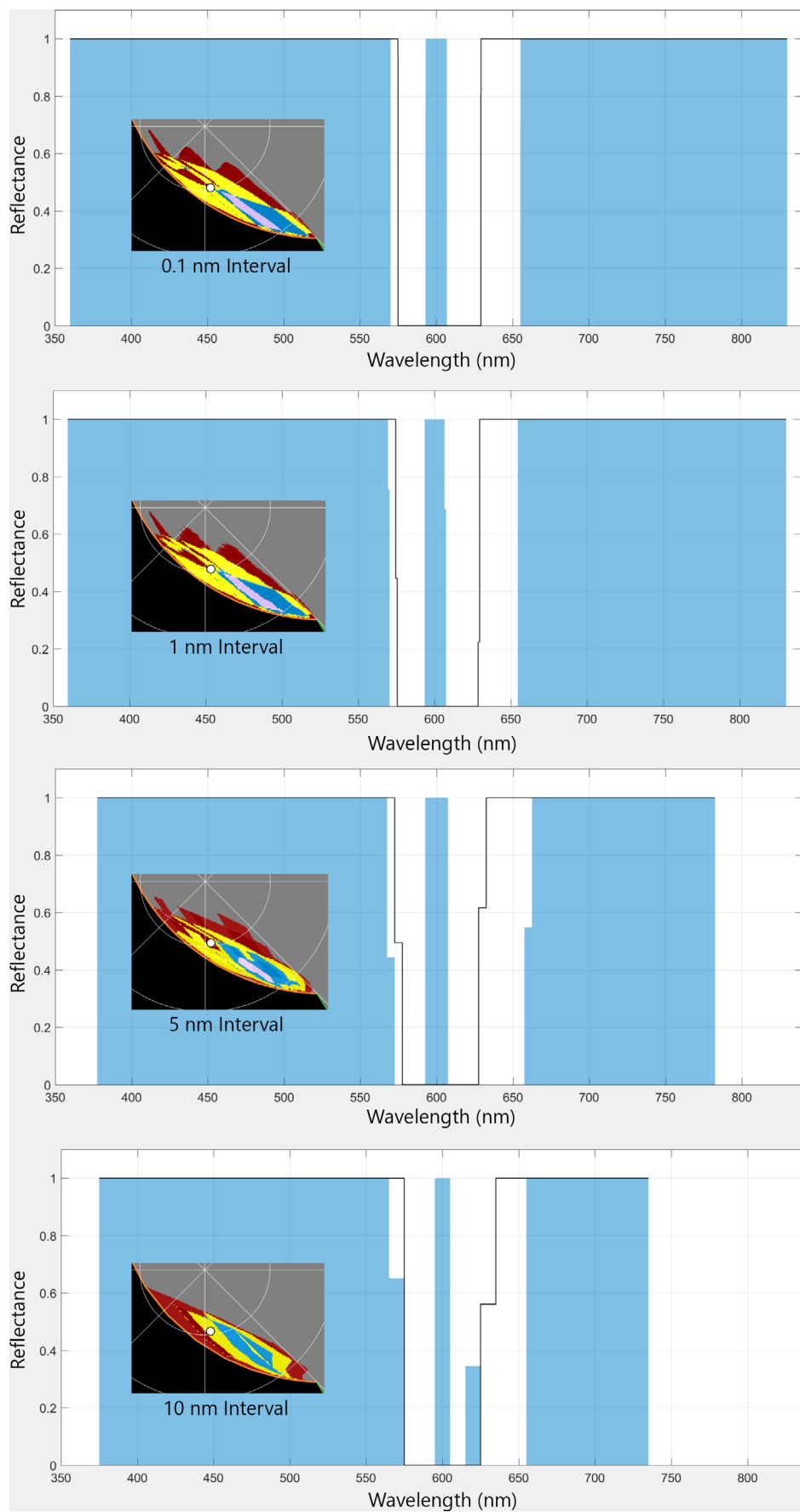
They are all shown at the top of Figure 9, scaled to have a maximum value of 1.

The lower portion of Figure 9 shows the regions of high-transition optimal colors associated with each of the Munsell-based illuminants, plotted on the chromaticity plane. The small circles are the chromaticities of the illuminants. The green and orange lines are the main and opposite meridians. Only the type II-like regions appear since the type I-like regions have very high chromatic purity, and are compressed along the boundary of the chromaticity diagram. It is evident that the general distribution of transition count locations persists across a wide range of illuminants. The choppiness in Figure 9 is simply an artifact of a difference in graphics resolution between Figures 6 and 9.
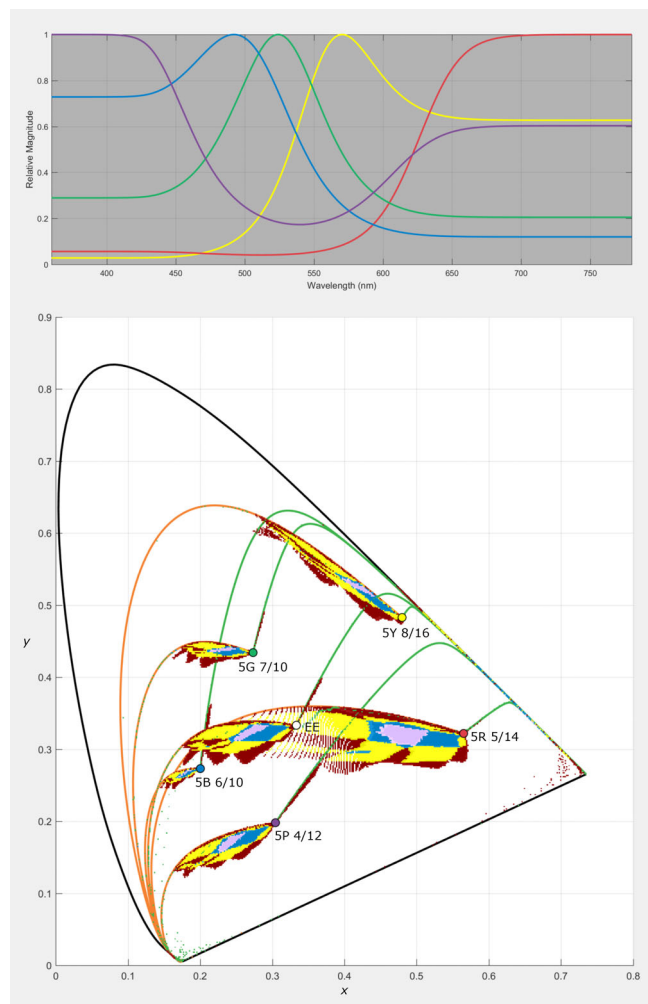

FIGURE 9 (Top) Five illuminants with chromaticities matching Munsell 5R 5/14, 5Y 8/16, 5G 7/10, 5B 6/10, and 5P 4/12. (Bottom) High-transition optimal color regions associated with each illuminant, plotted on the chromaticity diagram

8 | IDENTIFYING THE SOURCE OF HIGH-TRANSITION OPTIMAL COLORS

This section examines which portions of the chromaticity diagram are the most responsible for the high-transition optimal colors. As mentioned in Section 2, the non-convexity along the nearly straight, right-hand side of the chromaticity diagram is very slight. What is not visible in Figure 1 is the behavior at both the far blue and far red ends of the chromaticity diagram. At the far blue end, the chromaticity diagram points between 360 and 412 nm make several excursions away from the convex hull boundary and into the interior of the convex hull. The largest of these excursions is about three times larger than what was shown in Figure 1 inset (0.00013 vs 0.00005 in chromaticity space units).

The far red end shows a much different behavior. Beyond a wavelength of 699 nm, the points on the chromaticity diagram begin to zigzag back and forth along a fairly straight line in x, y space. This zigzag behavior is clearly observed in Figure 10 when the distribution of chromaticity diagram coordinates, x and y, are plotted separately against wavelength.

To assess what impact these far-end non-convexities have on the high-transition optimal object colors, the two ends of the CMFs were removed, leaving only the values for wavelengths 412 to 699 nm. The computation that produced Figure 6 was repeated for the truncated CMFs and the results are shown on the right side of Figure 11, with a comparison to the original Figure 6 results shown on the left side of the figure. It is evident that the far-end non-convexities have little impact on the distribution of high-transition optimal object colors.

9 | CONVEXIFYING THE CMFs

One final experiment was performed on the truncated 1931 2° CIE CMFs (412-699 nm portion). Centore suggested it might be interesting to perturb the values of the CMFs slightly to move the slightly non-convex members of the chromaticity diagram onto the convex hull boundary.[27] One way to do this "convexification" is demonstrated in Figure 12.

The convexification algorithm proceeds as follows: First, we identify a pair of chromaticity coordinates that belong to the convex hull boundary (the black dots in Figure 1) that enclose one or more points not on the boundary (the red dots in Figure 1). For example, the "black" points at wavelengths 574 and 612 nm enclose 37 "red" points not on the convex hull boundary (575-611 nm). Then, we mathematically construct a
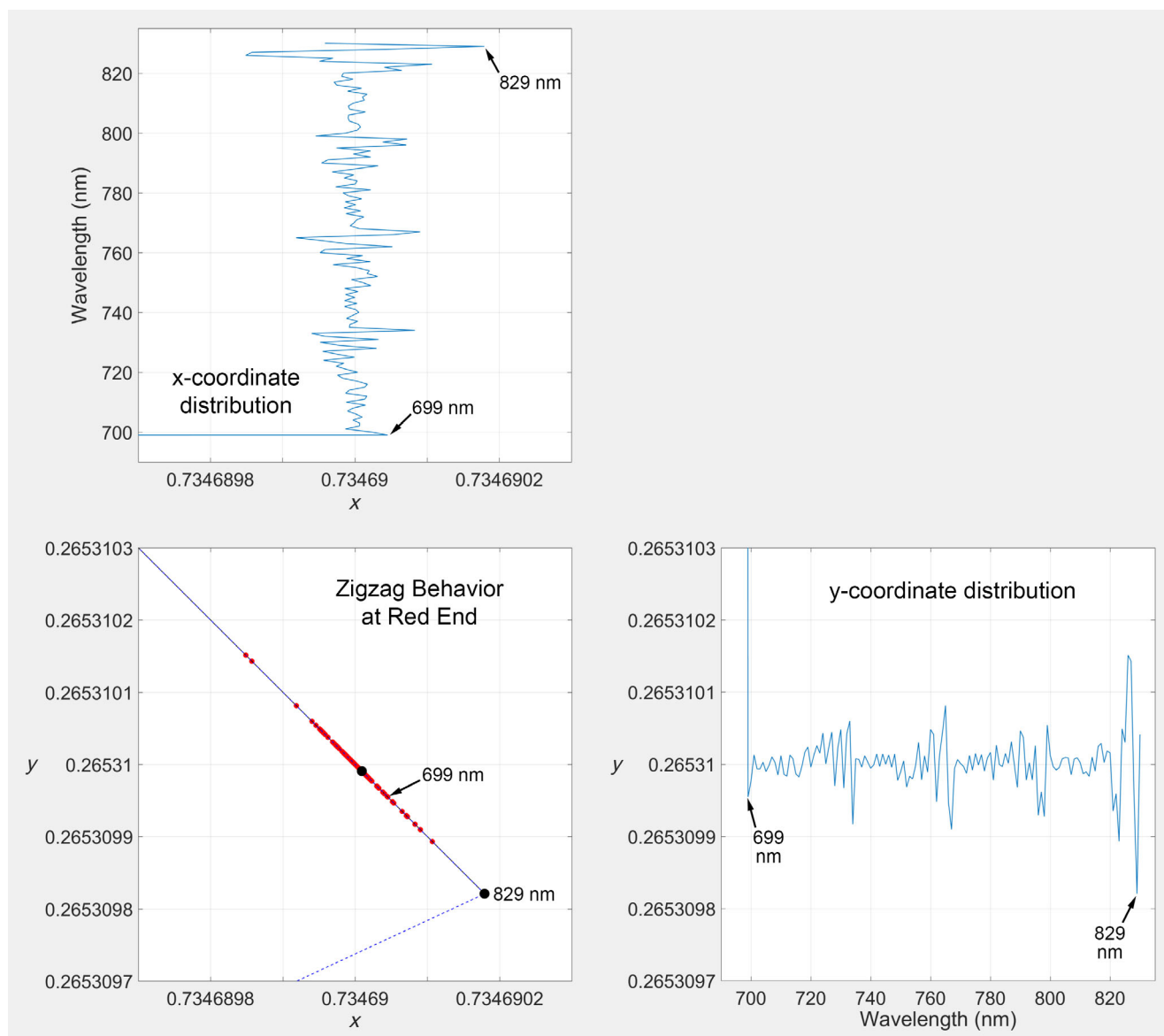
FIGURE 10 Behavior of the far red end of the 1931 2° CIE chromaticity diagram, showing zigzag behavior beyond 699 nm
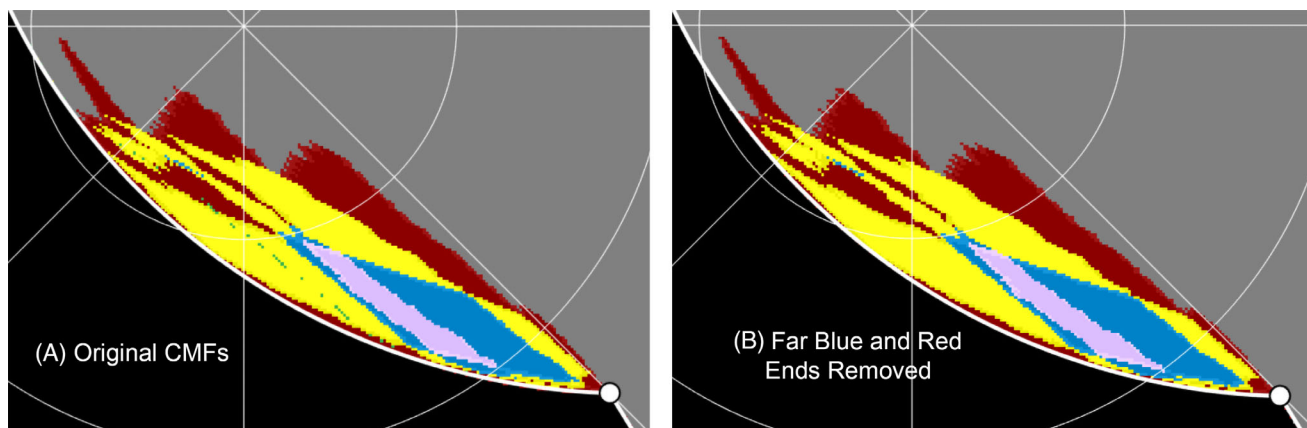

FIGURE 11 The minimal effect on high-transition optimal object colors after removing the far blue and red ends of the color-matching functions

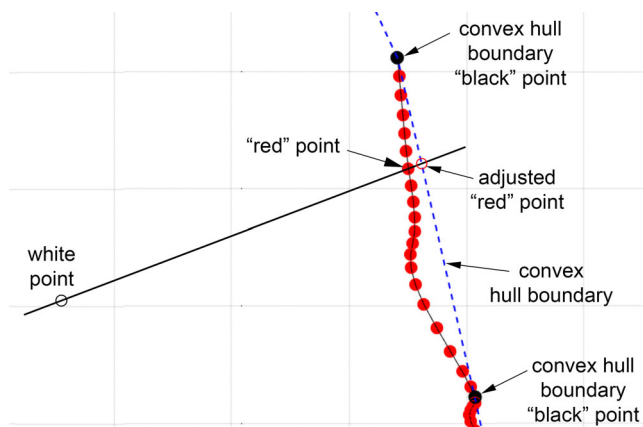straight line that connects the two black convex hull points. Now for each interior red point, we construct another line that passes through the red point and the central white point of the chromaticity diagram. The intersection of these two lines will have slightly different (x, y) coordinates than those of the red point. We can convert these modified x and y values (along with the original Y value of the red point) to tristimulus values, XYZ, and replace the corresponding row of the CMFs with the adjusted values. We repeat this for each red point between the two enclosing black convex hull points. This creates a straight line of modified red points that align with the convex hull boundary. Finally, we repeat this entire process for all remaining pairs of black points that enclose one or more red points.

The outcome of the convexification process is a set of CMFs that produce a chromaticity diagram that is convex and also well-ordered in wavelength (because the far red end was previously removed). Thus, the convexified CMFs satisfy West and Brill's conditions under which Schrödinger (two-transition) colors are optimal.[9] The computation that produced Figure 6 was again repeated
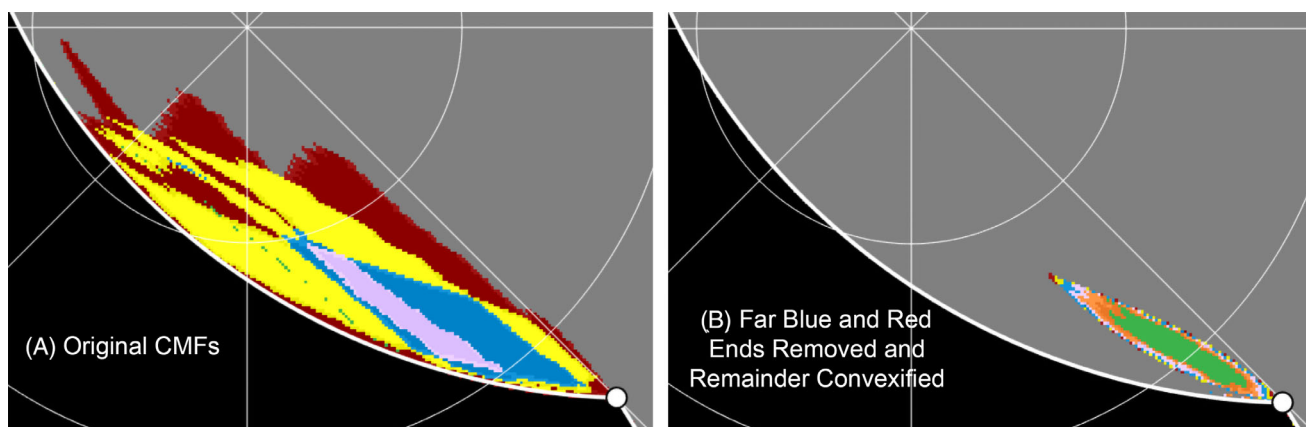

FIGURE 12 Convexification of the chromaticity diagram

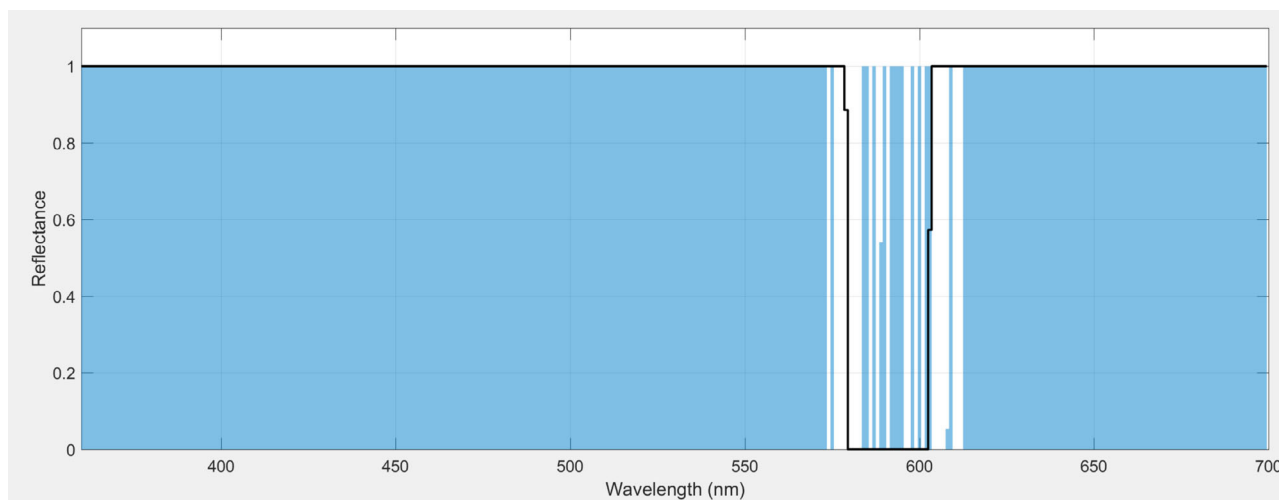**FIGURE 13** High-transition optimal object color locations after convexification

FIGURE 14 A 20-transition optimal object color linear programming solution (blue-filled bar plot) and a metameric two-transition Schrödinger color (black-outlined bar plot)

for the convexified CMFs, and the results are shown on the right side of Figure 13, with a comparison to the original results of Figure 6 shown on the left side of the figure.

The region of high-transition optimal object colors has diminished substantially, but still remains. The transition count for this remaining region is higher than before; the color coding is as follows: maroon = 4 transitions, yellow = 6 transitions, blue = 8 transitions, lavender = 10 transitions, orange = 12 to 14 transitions, green = 16 to 24 transitions. A sample reflectance curve from the green region (with 20 transitions) is shown in Figure 14, along with the Schrödinger two-transition reflectance curve along the same XYZ_{targ} target direction computed from the Masaoka & Berns algorithm.

Upon closer examination, it is found that the distance from $XYZ_{50\%}$ to each of the two colors shown in Figure 14 matches to machine floating point precision. They also share the same tristimulus values to machine precision. It is reasonable to conclude that the two colors are metamers of one another and both reside at the same point on the surface of the OCS. This conclusion also agrees with West and Brill's conditions mentioned earlier, since the two-transition color is optimal, even though it shares a metameric match with another color that has a higher transition count.

One way to interpret this result is to refer back to the early article by Schrödinger.[1] Brill, in his technical introduction to Kuehni's English translation of that article,[28] notes that Schrödinger went to great lengths to discuss the effect of having a linear portion of the chromaticity diagram. Schrödinger concluded there is a possibility of optimal metamers with more than two transitions arising from the linear portion. It is possible that this phenomenon is what gives rise to the metameric optimal object colors observed in Figure 13.

10 | MODERN CMFs

So far, this presentation has focused on the 1931 2° CIE CMFs. It is natural to wonder if the same high-transition optimal object color phenomena are shared by other, more modern versions of CMFs. We now turn to a recently-proposed set of CMFs transformed from the cone fundamentals of Stockman and Sharpe,[29] also known as "physiologically-relevant" CMFs.[11] Examining the convex hull enveloping the chromaticity diagram derived from these CMFs, it is found that some slight non-convexity persists along the nearly linear right-hand side, but the inward deviation from the convex hull boundary is about 30 times smaller than that observed with the 1931 CMFs, measured in chromaticity space. The far blue end also shows some significant non-convexity for points
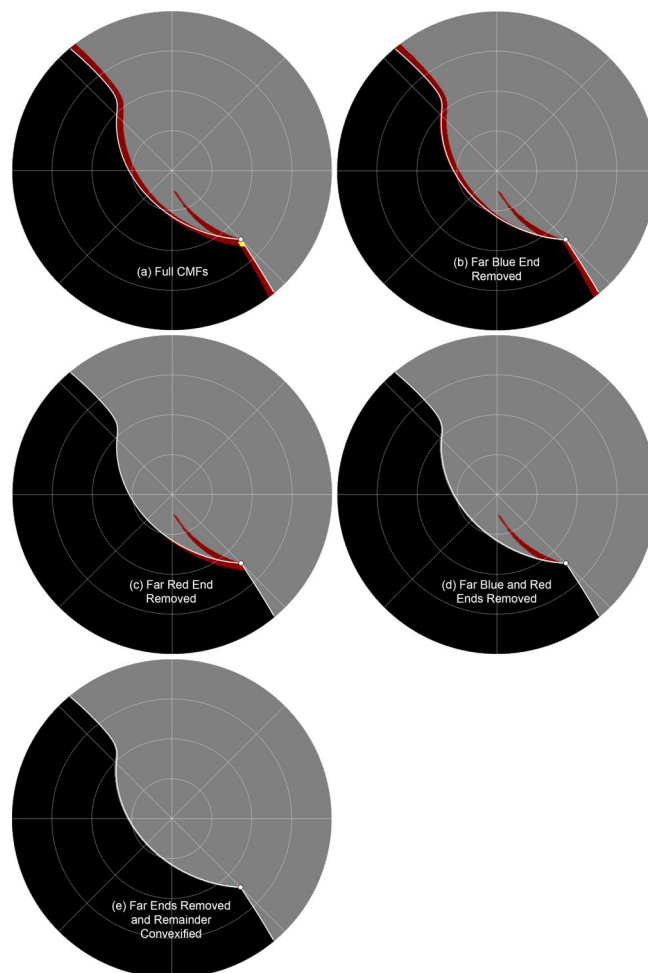

FIGURE 15 Higher-transition optimal object colors produced by physiologically relevant color-matching functions, with and without far ends removed and convexified (see text)

<410 nm. The far red end does not experience the zigzag behavior of the 1931 CMFs. Instead, the chromaticity diagram makes a 180° reversal in direction at 703 nm and continues to back up along the same curve for points >703 nm, with the final endpoint of 830 nm landing between the points 647 and 648 nm.

The computation that produced Figure 6 was performed for the modern CMFs in several different ways, all summarized in Figure 15. In each case, only the top half is shown since the lower half is again a point-symmetric copy. The meridians are shown as heavy white lines and the white point is shown as a white circle. In the first image (a), the unmodified CMFs are examined, showing that there are some regions of higher transition count, mostly along the meridians, but also along a narrow wisp extending away from the meridians. The transition count is four in the maroon region and six in the small yellow region. Next, two modifications of the CMFs are examined, image (b) which removes the far blue end <410 nm, and image (c) which removes the far red end >703 nm. Next, both the far blue

and far red ends are removed in image (d). At this point, the only remaining region of higher-transition count is the narrow wisp that extends away from the meridians. We can conclude that the higher-transition count region along the meridians is due to the behavior of the far ends of the chromaticity diagram, because it disappears when the far ends of the CMFs are removed.

Figure 15E is the result of applying the convexification procedure discussed in Section 9 to the truncated CMFs having both far blue and red ends removed. The resulting CMFs produce a chromaticity diagram that is convex and well-ordered in wavelength. All instances of higher-transition colors are eliminated by the convexification; all optimal object colors are now of the two-transition Schrödinger type. It is interesting to note that we do not see any high-transition colors appearing due to the linear portions produced by the convexification process, as we saw with the 1929 CMFs. It is not clear why this is, and this could be the subject of further inquiry.

11 | CONCLUSIONS

The main conclusion that can be drawn from this presentation is that very slight non-convexities of the spectrum locus can have a significant impact on the shape of reflectance curves associated with optimal object colors. For the 1931 2° CIE CMFs, there are regions on the surface of the OCS containing optimal object colors with transition count higher than the usual two-transition Schrödinger colors. There are still two-transition colors that exist very near these high-transition colors, but they are located slightly toward the interior of the OCS, and are therefore not optimal.

Another interesting observation is that the high-transition solutions appear to come in point-symmetric pairs, one type I-like and the other type II-like, but otherwise matching in transition count and transition locations. The size of the regions of high-transition optimal colors, when plotted on the chromaticity diagram, depends on the illuminant. The largest regions are associated with illuminants nearest to the boundary non-convexity.

A convexification procedure was developed and applied to the CMFs to slightly perturb the chromaticity diagram to become convex. It causes several segments of the chromaticity diagram to become linear, which appears to generate high-transition optimal object colors that are metameric to two-transition Schrödinger optimal object colors, as predicted by Schrödinger in his 1920 article.

More modern CMFs were examined and instances of higher-transition optimal object colors are nearly absent. Most of them arise from the non-convexity at the far ends of the chromaticity diagram, and the remaining ones are extinguished by convexifying the CMFs.

The use of LP to find optimal reflectance spectra is not new, but the way of searching along an arbitrary ray through a target is unique. This brings up other potential applications. For example, to create a slice of the three-dimensional OCS for some fixed value of X, Y, or Z, all we need to do is relocate our coordinate system to the point on the gray line (connecting the origin and the white point) that has the desired value of X, Y, or Z, and then sweep the search ray around a circle in the plane of the other two tristimulus coordinates.

Additional supporting material and additional discussion can be found in the online supplementary documentation of this article.[30]

ORCID
Scott A. Burns https://orcid.org/0000-0002-1251-7758

ENDNOTE
* There is a very minor bug in the Masaoka & Berns MATLAB code. The statement in their function "optm" XYZopt = sum($T(L(1):L(2),:)$)... should be instead XYZopt = sum($T(L(1):L(2),:),1$).... The bug occurs in the very rare instance when $L(1) = L(2)$; in that case, the original statement incorrectly returns a scalar.

REFERENCES
[1] Schrödinger E. Theorie der pigmente von grösster leuchtkraft. *Ann Phys*. 1920;62:603-622.

[2] MacAdam DL. The theory of the maximum visual efficiency of colored materials. *J Opt Soc Am*. 1935;25(8):249-252.

[3] MacAdam DL. Maximum visual efficiency of colored materials. *J Opt Soc Am*. 1935;25(11):361-367.

[4] Wyszecki G, Stiles WS. *Color Science, Concepts and Methods, Quantitative Data and Formulae*. 2nd ed. New York, NY: John Wiley & Sons; 1982:179-184.

[5] MacAdam DL. *Color Measurement, Theme and Variations*. 2nd ed. Berlin Heidelberg New York, NY: Springer-Verlag; 1985:122.

[6] Koenderink JJ, van Doorn AJ. Perspectives on colour space. In: Mausfeld R, Heyer D, eds. *Colour Vision: from Light to Object*. Oxford, UK: Oxford University Press; 2003:1-56.

[7] Kuehni RG. *Color, an Introduction to Practice and Principles*. 3rd ed. Hoboken, NJ: John Wiley & Sons; 2013:126.

[8] Oleari C. *Standard Colorimetry, Definitions, Algorithms and Software*. Chichester, West Sussex, UK: John Wiley & Sons; 2016:352.

[9] West G, Brill M. Conditions under which Schrödinger object colors are optimal. *J Opt Soc Am*. 1983;73(9):1223-1225.

[10] Davis G. Convexity and Transitions, A Strict Examination of the 1931 CIE inverted-U. 2020 https://cran.r-project.org/web/packages/colorSpec/vignettes/convexity.pdf. Accessed March 26, 2021.

[11] University College London, Color & Vision Research Laboratory. Color Matching Functions http://cvrl.ioo.ucl.ac.uk/cmfs.htm. Accessed March 3, 2021.

[12] Rochester Institute of Technology, Munsell Color Science Laboratory. Useful Color Data https://www.rit.edu/cos/colorscience/rc_useful_data.php; Short URL https://bit.ly/39hBp4e; Excel data at http://www.rit-mcsl.org/UsefulData/all_1nm_data.xls; Short URL: https://bit.ly/3srkdAL. Accessed March 26, 2021.

[13] Martínez-Verdú F, Perales E, Chorro E, de Fez D, Viqueira V, Gilabert E. Computation and visualization of the MacAdam limits for any lightness, hue angle, and light source. *J Opt Soc Am A*. 2007;24(6):1501-1515.

[14] Allen E. Some new advances in the study of metamerism: theoretical limits of metamerism; an index of metamerism for observer differences. *Color Eng*. 1969;7(1):35-40.

[15] Ohta N, Wyszecki G. Theoretical chromaticity-mismatch limits of metamers viewed under different illuminants. *J Opt Soc Am*. 1975;65(3):327-333.

[16] Centore P. An Open-Source Algorithm for Metamer Mismatch Bodies. 2021 https://www.munsellcolourscienceforpainters.com/ColourSciencePapers/AnOpenSourceAlgorithmForMetamerMismatchBodies.pdf; Short URL: https://bit.ly/3fhUBCK Accessed March 26, 2021

[17] Mackiewicz M, Rivertz HJ, Finlayson G. Spherical sampling methods for the calculation of metamer mismatch volumes. *J Opt Soc Am A*. 2019;36(1):96-104.

[18] Ohta N, Wyszecki G. Designing illuminants that render given objects in prescribed colors. *J Opt Soc Am*. 1976;66(3):269-275.

[19] Allen E. Basic equations used in computer color matching. *J Opt Soc Am*. 1966;56(9):1256-1259.

[20] Belanger PR. Linear-programming approach to color recipe formulations. *J Opt Soc Am*. 1974;64(11):1541-1544.

[21] Cogno JA, Jungman D, Conno JC. Linear and quadratic optimization algorithms for computer color matching. *Color Res Appl*. 1988;13(1):40-42.

[22] Li C, Luo MR, Cho MS, Kim JS. Linear programming method for computing the gamut of object color solid. *J Opt Soc Am A*. 2010;27(5):985-991.

[23] Masaoka K, Berns RS. Computation of optimal metamers. *Opt Lett*. 2013;38(5):754-756.

[24] Logvinenko AD. An object-color space. *J Vision*. 2009;9(11):1-23.

[25] Burns SA. Numerical methods for smoothest reflectance reconstruction. *Color Res Appl*. 2020;45(1):8-21.

[26] Burns SA. Chromatic adaptation transform by spectral reconstruction. *Color Res Appl*. 2019;44(5):682-693.

[27] Centore P. Private Communication. 2021.

[28] Kuehni RG. Erwin Schrödinger, Theorie der Pigmente von grösster Leuchtkraft (Theory of pigments of greatest lightness). http://www.iscc-archive.org/pdf/SchroePigments2.pdf Also: https://web.archive.org/web/20190120185844/http://www.iscc-archive.org/pdf/SchroePigments2.pdf Short URL: https://bit.ly/39fUdkv Accessed March 26, 2021 2021.

[29] Stockman A, Sharpe L. The spectral sensitivities of the middle- and long-wavelength-sensitive cones derived from measurements in observers of known genotype. *Vision Res*. 2000;40:1711-1737.

[30] Burns SA. Supplementary Documentation: The Location of Optimal Object Colors with More Than Two Transitions, http://scottburns.us/ocss_suppl_docs/ Accessed March 26, 2021 2021.

AUTHOR BIOGRAPHY

Scott A. Burns is an engineering professor (now Emeritus) at the University of Illinois at Urbana-Champaign (UIUC). He has been interested in color science since the 1980s, when he was introduced to the topic by his colleague Jozef Cohen, with whom he and another colleague, Edward Kuznetsov, published papers on Fundamental Color Space and Matrix-R Theory. His other research interests include engineering design optimization, structural design, mechanism design, mechatronics, numerical methods, and data visualization. He received a National Science Foundation Presidential Young Investigator award in 1989, a UIUC College of Engineering Everitt Award for Teaching Excellence in 1990, was named a fellow in the UIUC Center for Advanced Study in 1992, and received two State-of-the-Art in Civil Engineering Awards from ASCE in 1998 and 2004. He retired from UIUC in 2009 but remains active in research activities and in advising student teams as part of the senior design capstone experience.